JℲM RAPIDS

Experiments on water-wave interactions with a horizontal submerged elastic plate

Gatien Polly,[1] **Alexis Mérigaud**[1,2] ⬤, **Benjamin Thiria**[1] **and Ramiro Godoy-Diana**[1] ⬤

[1]Laboratoire de Physique et Mécanique des Milieux Hétérogènes (PMMH), CNRS UMR 7636, ESPCI Paris–Université PSL, Sorbonne Université, Université Paris Cité, 75005 Paris, France
[2]IFP Energies Nouvelles, 92852 Rueil-Malmaison, France
Corresponding author: Ramiro Godoy-Diana, ramiro@pmmh.espci.fr

This article explores how a submerged elastic plate, clamped at one edge, interacts with water waves. Submerged elastic plates have been considered as potentially effective design elements in the development of wave energy harvesters but their behaviour in a wave field remains largely unexplored, especially experimentally. Positioned at a fixed depth in a wave tank, the flexible plate demonstrates significant wave reflection capabilities, a characteristic absent in rigid plates of identical dimensions. The experiments thus reveal that plate motion is crucial for wave reflection. Sufficiently steep waves are shown to induce a change in the mean position of the plate, with the trailing edge reaching the free surface in some cases. This configuration change is found to be particularly efficient to break water waves. These findings contribute to understanding the potential of elastic plates for wave energy harvesting and wave attenuation scenarios.

Key words: wave-structure interactions, coastal engineering

1. Introduction

The potential of wave energy as a renewable electricity source has been assessed to exceed the global demand for electricity (Sheng 2019; Mork *et al.* 2010). However, efficient designs still remain to be developed at an industrial level. Horizontally submerged flexible plates could be part of those designs due to their improved survivability (Collins *et al.* 2021). Until now, flexible submerged elastic plates have mostly been studied numerically and theoretically in a configuration where both edges are clamped, with the objective of

G. Polly, A. Mérigaud, B. Thiria and R. Godoy-Diana

harnessing wave energy or protecting the coastline. Cho & Kim (1998) and Cho & Kim (2000) considered the plate as a potential wave barrier. From the on-site observations that a muddy seafloor can effectively dampen water waves, Alam (2012) proposed a design to harvest wave energy by mimicking this phenomenon. To that aim, a flexible plate is used as a wave energy harvester. The flexible plate is hinged at the seafloor and oscillates due to the wave forcing, similarly to the mud in the ocean floor. Those oscillations are used to produce electricity by means of a power take-off (PTO) system. The Wave-Carpet design has been investigated numerically and experimentally by Desmars *et al.* (2018), Asaeian *et al.* (2020) and Lehmann *et al.* (2013). Renzi (2016) studied numerically a variation of the Wave-Carpet considering the use of a piezoelectric material to produce electricity, while Achour *et al.* (2020) added the effect of a current in addition to the waves. Boral *et al.* (2023) investigated the case of a flexible thin submerged plate resting on an elastic foundation modelled using the Winkler approach. Finally, submerged flexible plates clamped at both edges have been studied in more complex configurations, such as close to a wall as potential wave barriers (Guo *et al.* 2020; Gayathri *et al.* 2020; Mohapatra & Guedes Soares 2020), superimposed with other plates (Mohapatra & Sahoo 2014; Mohapatra & Guedes Soares 2019; Behera 2021; Das *et al.* 2020) or in series (Mirza & Hassan 2024*a*,*b*).

Contrary to the two-edge clamping, clamping the plate at only one edge has barely been studied. Shoele (2023) investigated numerically the case of a submerged elastic plate as a hybrid current/wave energy converter but the impact of waves alone was not examined. Michele *et al.* (2020) investigated the behaviour of a floating elastic plate moored onto a set of PTO systems. Their theoretical model shows that plate elasticity introduces additional resonant frequencies compared with rigid plates, enhancing both wave energy extraction and the capture factor bandwidth. While their preliminary experimental estimations of power extraction with a flexible floater demonstrator compared favourably with their model, the wave–structure interaction mechanisms remain largely unexplored.

The aim of this paper is to characterize experimentally the interaction of a flexible submerged elastic plate, clamped at only one edge, with water waves. A table-top experiment has been developed to study the wave–plate interaction, which allows the use of vision-based data extraction techniques. Schlieren imaging is utilized to measure the free-surface height and a side view of the tank to track the plate deformation. The ability of the plate to reflect, transmit or dissipate water waves is computed measuring the reflection and transmission coefficients. It is observed that the flexible plate can reflect water waves over a certain range of waves frequencies. It exposes potential applications of such a system for coastal protection and, more generally, offers a deeper fundamental understanding of the role played by flexibility in the wave–structure interaction applications. The comparison of wave reflection and transmission by a submerged flexible plate and a submerged rigid plate of the same dimensions shows that the plate motion is responsible for wave reflection. Finally, when increasing the wave amplitude, the flexible plate can act like a perfect wave absorber by changing its mean position. The flexible plate acts as a reconfigurable water-wave absorber which could be able to totally dampen the waves in high sea conditions.

2. Experimental methods

2.1. *Experimental set-up*

The experimental set-up is represented in figure 1(*a*), in a reference frame with *x* the direction of propagation of the waves, *y* the transverse direction, and *z* the vertical coordinate, respectively. The total length of the tank is 2.5 m, where the measurement
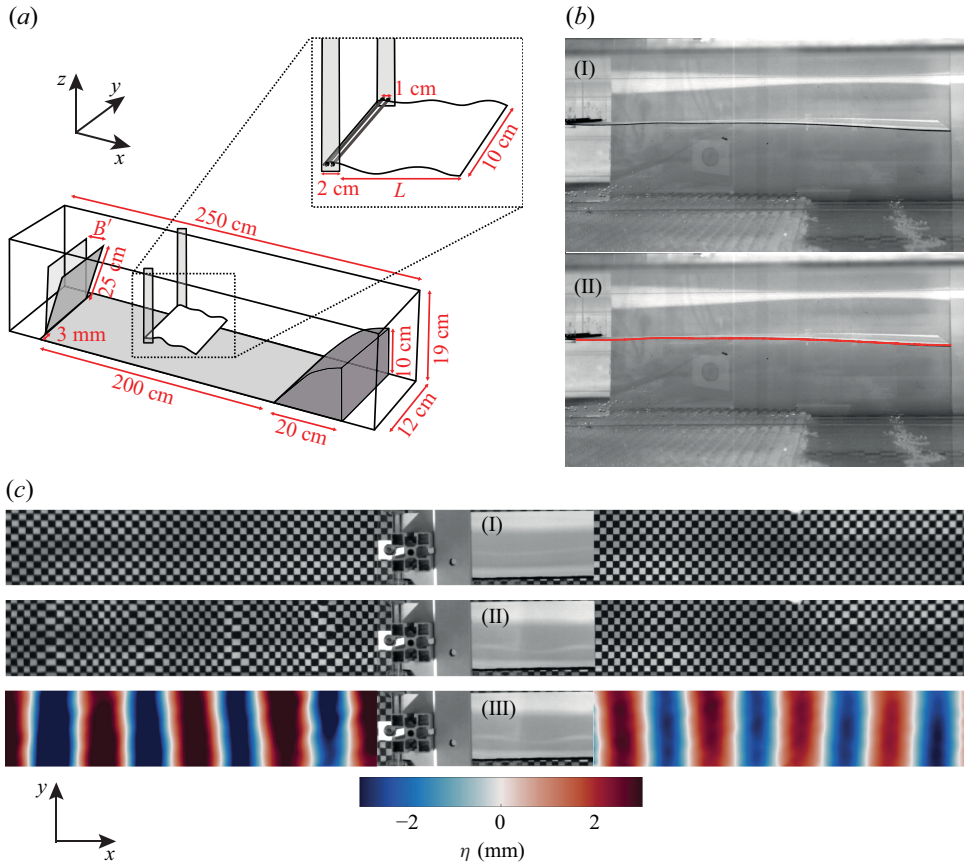
Figure 1. (*a*) Schematic diagram of the experimental set-up. The plate length L is 28 cm. (*b*) Side view of the tank with the plate: picture (I) is a raw image while picture (II) illustrates the detected edge of the plate (red line). (*c*) Tank top view: picture (I) is taken with an undisturbed free surface. For picture (II), 3.5 Hz/13 cm waves of 3 mm amplitude are generated and the chequerboard appears deformed. The bottom picture illustrates the free-surface height reconstruction using Schlieren imaging.

region is 2 m long at the centre of the tank. The tank width is restricted to a 12 cm channel to prevent transverse modes in the investigated range of frequencies (Ursell 1952). Water depth is fixed at 10 cm. Waves are produced using a flap type wave-maker driven by a linear motor (DM 01-23x80F-HP-R-60_MS11 from Linmot®). In practice, the waves produced in this set-up have an amplitude ranging from 0.5 to 5 mm and frequencies ranging from 1.5 to 4 Hz. The wave angular frequency, ω, is related to the wavenumber, k, through the dispersion relation of gravity waves:

$$\omega^2 = gk \tanh(kh), \qquad (2.1)$$

where g is the acceleration of gravity and h the water depth. The studied wavelengths, λ, range from 10 to 55 cm, so that λ/h ranges from 1 to 5.5, corresponding to deep to intermediate water depths. The plate is positioned halfway through the tank length at $x = 0$ m. At the end of the tank, a parabolic beach is placed. It is used to limit reflection on the tank wall (Ouellet & Datta 1986). The beach is pierced with 5 mm circular holes to enhance viscous damping. Data are extracted from this set-up by filming simultaneously from the

top and the side of the tank, giving access to the free-surface deformation and the plate motion.

2.2. *Water-wave height measurements*

The free-surface deformation is computed using Schlieren imaging (Moisy *et al.* 2009; Wildeman 2018). To do so, a chequerboard pattern is placed at the bottom of the tank. When waves propagate, the image of the chequerboard obtained by filming with the top camera appears to be deformed, as illustrated in figure 1(*c*). Both figures 1(*c*) (I) and (II) show an image taken by the top camera with the plate placed in the middle of the tank. In (I), no waves are propagating, whereas in (II) 3.5 Hz/13 cm waves of 2.5 mm amplitude are propagating in the tank. The comparison between those two images is used to reconstruct the free-surface height in all the tank by using the open-source code provided by Wildeman (2018). Figure 1*(c)* (III) illustrates free-surface reconstruction using images (I) and (II). The tank can be divided into two different regions: the up-wave region, located between the wave-maker and the plate, where the incoming wave, produced by the wave-maker, and the wave reflected by the plate propagate; and the down-wave region, located between the plate and the beach, where waves transmitted by the plate propagate, as well as a small component of waves reflected from the absorption beach. After filtering at the wave-maker angular frequency, ω, the free-surface elevation can be described as the sum of two waves propagating forward and backward in each region:

$$\begin{cases} \eta^{uw}(x,t) = \mathrm{Re}(\hat{\eta}_+^{uw}(x)e^{-i\omega t} + \hat{\eta}_-^{uw}(x)e^{-i\omega t}) \text{ with } \hat{\eta}_\pm^{uw}(x) = \hat{A}_\pm^{uw}e^{\pm(ik-\nu)x} \\ \eta^{dw}(x,t) = \mathrm{Re}(\hat{\eta}_+^{dw}(x)e^{-i\omega t} + \hat{\eta}_-^{dw}(x)e^{-i\omega t}) \text{ with } \hat{\eta}_\pm^{dw}(x) = \hat{A}_\pm^{dw}e^{\pm(ik-\nu)x}, \end{cases} \tag{2.2}$$

where η is the free-surface height and the superscripts *uw* and *dw* stand for up-wave and down-wave, respectively. Quantities associated with waves propagating forward and downward are indicated using the subscripts $+$ and $-$, respectively, and complex numbers are denoted using the symbol ˆ. Here $\hat{\eta}$ is the complex spatial part of the free-surface height (it depends on k the wavenumber), $\hat{A}$ the complex wave amplitudes, and ν a damping coefficient that models wave dissipation along the tank.

The energy reflection and transmission coefficients, K_r and K_t, for a given wave amplitude and frequency are defined as

$$K_r = \left(\frac{|\hat{A}_-^{uw}|}{|\hat{A}_+^{uw}|} \right)^2 \text{ and } K_t = \left(\frac{|\hat{A}_+^{dw}|}{|\hat{A}_+^{uw}|} \right)^2. \tag{2.3}$$

To determine the reflection and transmission coefficients, the amplitude of the waves propagating forward and backward have to be measured. The image deformation is related to the free-surface height by (Moisy *et al.* 2009)

$$\nabla \eta = -\frac{\boldsymbol{u}}{h^*}, \tag{2.4}$$

where h^* is a real-valued parameter that depends on water depth and set-up configuration and $\boldsymbol{u}$ is the deformation field. The vector $\boldsymbol{u}$ has two components, u_x and u_y, corresponding to the image deformation along x and y. Generally, η is obtained by numerically inverting the gradient. However, as the free-surface height is non-zero on the edges of the image, the determination of the integration constant leads to numerical errors. In this work, gradient inversion is avoided by using the monochromatic nature of the waves studied. The elevation gradient, $\nabla \hat{\eta}$, is reduced to a simple partial derivative along x. Equation 2.2, leads to

$$\nabla \hat{\eta}_+ = (ik - \nu)\hat{\eta}_+ \text{ and } \nabla \hat{\eta}_- = -(ik - \nu)\hat{\eta}_-. \tag{2.5}$$

The Fourier transform of u_x at the wave-maker frequency, $\hat{u}_x(x)$, can also be decomposed in its forward/backward components as

$$\hat{u}_x(x) = \hat{u}_{x+}e^{(ik-\nu)x} + \hat{u}_{x-}e^{(-ik+\nu)x}, \tag{2.6}$$

with

$$\hat{u}_{x+} = -(ik - \nu)h^*\hat{\eta}_+ \text{ and } \hat{u}_{x-} = (ik - \nu)h^*\hat{\eta}_-. \tag{2.7}$$

Therefore, for monochromatic waves, K_r and K_t can be computed using only the image deformation:

$$K_r = \left(\frac{|\hat{u}_{x-}^{uw}|}{|\hat{u}_{x+}^{uw}|}\right)^2 \text{ and } K_t = \left(\frac{|\hat{u}_{x+}^{dw}|}{|\hat{u}_{x+}^{uw}|}\right)^2. \tag{2.8}$$

The four deformation amplitudes are obtained by choosing an arbitrary set of positions x_i where $\hat{u}_x$ is evaluated. The different amplitudes and the damping coefficient are determined by solving the system

$$\begin{cases} \hat{u}_x(x_1) = \hat{u}_{x+}\exp(ikx_1 - \nu x_1) + \hat{u}_{x-}\exp(-ikx_1 + \nu x_1) \\ \vdots \\ \hat{u}_x(x_{\max}) = \hat{u}_{x+}\exp(ikx_{\max} - \nu x_{\max}) + \hat{u}_{x-}\exp(-ikx_{\max} + \nu x_{\max}), \end{cases} \tag{2.9}$$

using a nonlinear least-squares method.

Top- and side-view movies are taken simultaneously by following the same protocol. First, a picture of the undisturbed tank is taken, giving a reference image for the top and side view. Then waves are sent for one minute and fifteen seconds. The first minute is used to reach a steady state and data are acquired during the last 15 s.

2.3. *Plate characteristics and clamping system*

The plate is placed submerged as pictured in figure 1, at a fixed depth of 3 cm. The leading edge of the plate is maintained submerged using a clamping system composed of two carbon rods of 2 mm diameter that are glued to the edge of the plate. The rods are attached to the support poles on the sides of the tank, ensuring that the leading edge remains still. The plate material choice is particularly crucial. Indeed, since the plate trailing edge remains free, a small density difference with water will induce a deviation from the horizontal at rest. In practice, such deviation can be mitigated by using a relatively rigid material. The plate itself is made by cutting polypropylene sheets of density 1035 kg m^{-3} and stiffness $1.7 \times 10^{-3} \text{ N m}^2$.

Figure 1(b) (I) is taken from the tank side view and shows the plate when no waves are present. The plate edge is coloured in black to allow its tracking as illustrated in picture (II). As can be appreciated, the plate position is close to horizontal. The plate length, L, is fixed at 28 cm, which enables the testing of ratios L/λ ranging from 0.45 to 2.7. The plate resonance frequencies have been measured forcing the plate at a 3 cm depth. For forcing frequencies between 0.5 and 4 Hz, two resonance frequencies of the system are observed, corresponding to the second and third plate mode, at respectively $f_2 = 0.6$ Hz and $f_3 = 1.96$ Hz.
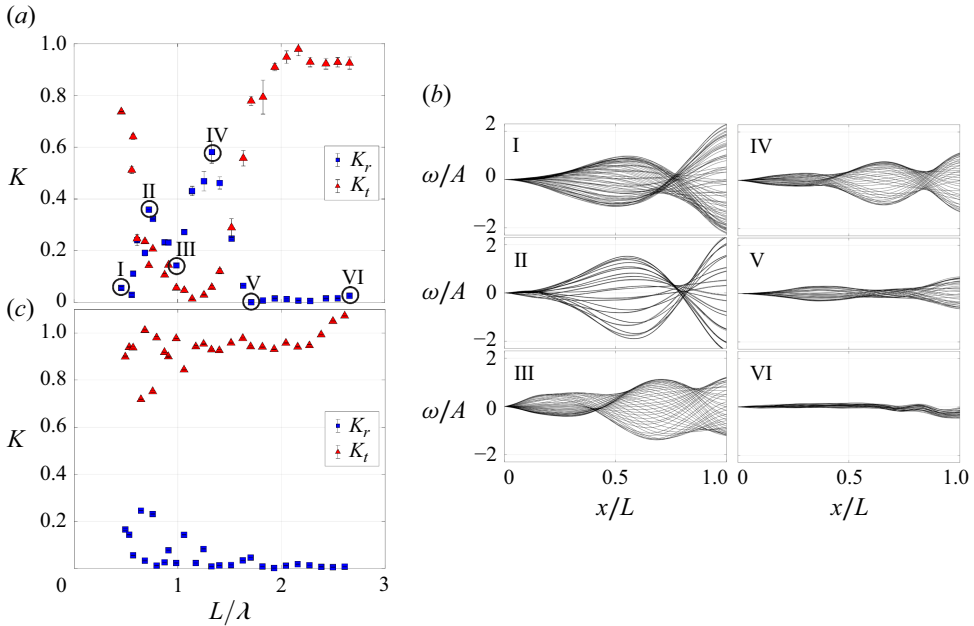
Figure 2. (*a*) Average over three experiments of the reflection and transmission coefficients, K_r (blue squares) and K_t (red triangles) for L/λ from 0.45 to 2.7. A significant reflection is observed for L/λ between 0.6 and 1.6 while for other values the plate mostly transmits waves. (*b*) Plate deflection w normalized by the incoming wave amplitude, A, for six values of L/λ indicated by I to VI in (*a*). Across the different values of L/λ, the plate amplitude of motion decreases and its deformation mode changes. (*c*) Reflection (blue squares) and transmission (red triangles) coefficients for a rigid plate of same dimensions as the flexible one. No reflection is observed, underlining the fact that the wave reflection is induced by the plate motion.

3. Results

3.1. *Low-wave-amplitude forcing*

Figure 2(*a*) shows the average, over three experiments, of the reflection and transmission coefficients, K_r and K_t, measured as a function of the ratio L/λ. These experiments were conducted with a water-wave amplitude of approximately 0.5 mm, which corresponds to the lowest wave amplitude that can be produced and effectively analysed. At lower values of L/λ, waves are mostly transmitted by the plate with the reflection coefficient, K_r, being almost equal to 0 for point (I). Increasing L/λ leads K_t to drop to 0 and K_r to rise to 60 % of the incoming wave energy (IV). For L/λ larger than 1.6, K_r drops again to 0 and the plate mostly transmits waves. It is observed that for $L/\lambda < 1.6$, $K_r + K_t < 1$, implying that a significant part of the incoming wave energy is dissipated. Figure 2(*b*) shows the plate deflection over one wave period, normalized by the incoming wave amplitude for different values of L/λ. When increasing L/λ, the plate amplitude of motion decreases. Also, when L/λ increases, the plate changes its deformation mode. It is illustrated by figure 2(*b*) (I) and (II) that have one node, while (III) and (IV) show two nodes. As illustrated by cases (V) and (VI), the values of L/λ, where the plate fully transmits water waves, is associated with almost no plate motion.

The reflection and transmission are also examined using a rigid plate made of aluminium having the same dimensions as the flexible plate. The corresponding K_r and K_t are presented in figure 2(*c*) as a function of L/λ. No reflection pattern is observed using a

rigid plate, highlighting the fact that the plate motion is necessary to reflect water waves in this case.

From a frequency perspective, the reflection zone is centred on 2.5 Hz (i.e. $f/f_2 = 4$ and $f/f_3 = 1.25$), covering frequencies between 1.8 and 3 Hz (i.e. $f/f_2 \in [3-5]$ and $f/f_3 \in [0.9-1.5]$).

3.2. *Large-wave-amplitude forcing*

Figures 3(*a*) and 3(*b*) illustrate the influence of the incoming wave amplitude, A_+, on the transmission and reflection coefficients, respectively. At lower L/λ, the wave amplitude has no influence on wave transmission by the plate. However, for larger L/λ, a drop in transmission is observed when A_+ increases. In terms of reflection, the increase in the incoming wave amplitude leads to an attenuation of the reflection peak. By interpolating all the experimental data points, we produce both the K_r and K_t maps in a wave-amplitude-L/λ space shown in figures 3(*c*) and 3(*d*). The lower amplitude case corresponds to data presented in § 3.1 with significant reflection for L/λ between 0.6 and 1.6. When increasing the wave amplitude, the reflection and transmission patterns are drastically modified. For $A_+ > 3$ mm, waves are neither reflected nor transmitted for $L/\lambda > 0.6$, meaning that the incoming wave energy is totally dissipated when interacting with the plate. This dissipation can be attributed to a change in the plate mean position for the $(A_+, L/\lambda)$ couples that are illustrated in figure 3. Figure 4(*a*) shows a picture taken from the side of the tank when conducting experiments for $A_+ = 6$ mm and $L/\lambda = 0.99$. The plate tip reaches the free surface under the effect of the waves. Similarly to a beach, this configuration is found to be particularly efficient to break water waves. The change in plate tip mean position, Δ_i, can be measured for all the experiments. Its values are presented in figure 4(*b*). The region where both K_r and K_t are equal to 0 corresponds to $\Delta_i/d \approx 1$, i.e. experiments for which the plate tip reaches the free surface. Figure 4(*c*) illustrates the correlation between the plate tip position and the part of the incoming wave energy that is dissipated, $1 - K_r - K_t$. The region where the plate tip reaches the free surface corresponds to the region where all the energy of the incoming wave is dissipated because of the interaction with the plate, i.e. $1 - K_r - K_t = 1$. For higher L/λ and lower amplitudes, no energy is dissipated, which is associated with regimes where the plate does not move.

4. Discussion and conclusion

The present study characterizes the interaction between a flexible plate, clamped at one edge, with water waves. It highlights experimentally that in such a configuration, the flexible plate can reflect wave energy. The comparison with a rigid plate enlightens the key role played by the plate's flexibility for potential coastal protection applications. The role of flexibility in structures intended for coastal protection has been largely discussed and is known to enhance wave dissipation compared with rigid structures (Kumar *et al.* 2007). However, the influence of flexibility on wave reflection remains generally unclear. For instance, Stamos & Hajj (2001) reported higher reflection coefficients for rigid submerged breakwaters. The present work highlights the opposite behaviour for a submerged elastic plate.

For this system, an uncommon physical process enhances wave dissipation. Owing to its ability to change its mean position when forced by the waves, the plate is passively placed in a configuration extremely efficient to break water waves. This configuration change, where the plate tip reaches the free surface, intervenes for the steepest water waves. The minimal steepness at which a significant change in position occurs is $A_+/\lambda \approx 10^{-2}$, for $A_+ = 3$ mm and $L/\lambda \approx 1$, which corresponds to slightly nonlinear waves (Le Méhauté
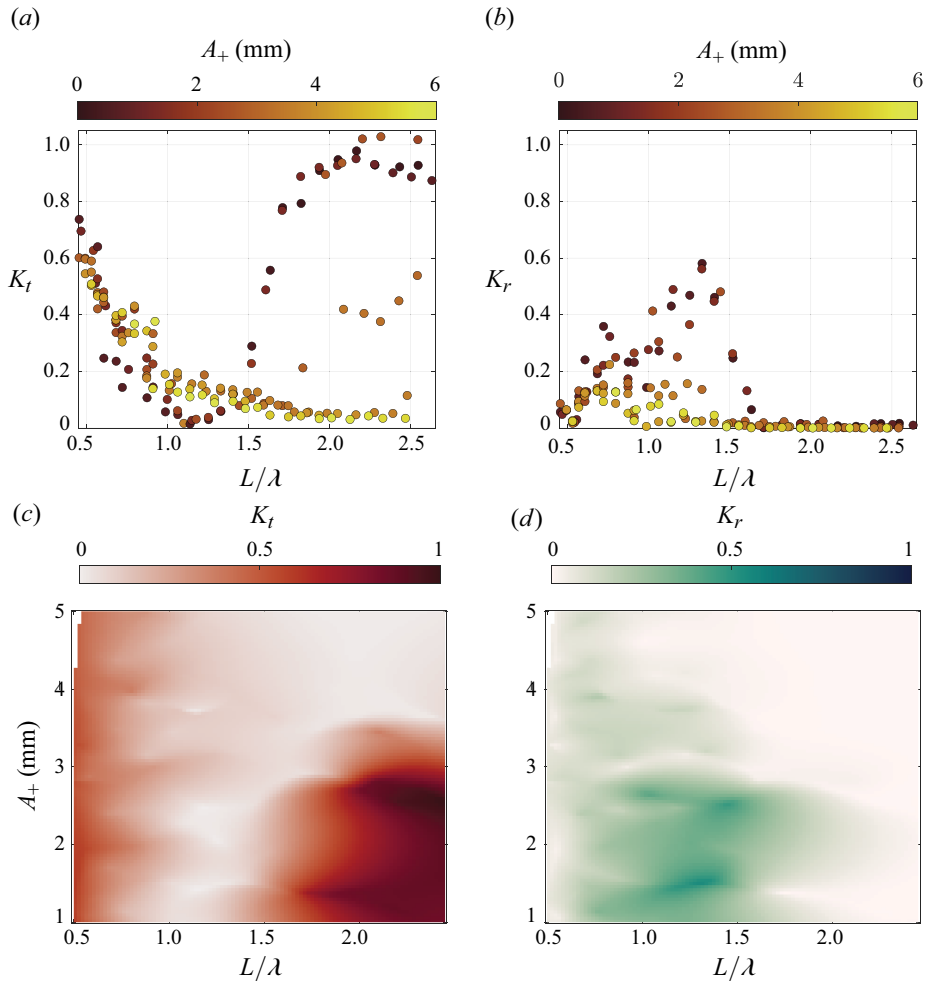
Figure 3. (*a*) Transmission coefficient, K_t, as a function of L/λ for six different wave amplitudes. The wave amplitude is indicated with different colours, from black to yellow, yellow corresponding to higher wave amplitudes. At low L/λ, the wave amplitude has a lower impact on K_t, while for high-amplitude waves, the transmission coefficient drops to zero. (*b*) Reflection coefficient, K_r, as a function of L/λ for six different wave amplitudes, using the same colour code as for the transmission coefficient. The increase in wave amplitude leads to a decrease in transmission. (*c,d*) The AvsL/λ diagrams showing the transmission (*c*) and reflection coefficients (*d*) interpolated using experimental data to cover the whole domain. Bright colours correspond to the coefficient being equal to 0 and dark colours to the coefficient equal to 1. For the steepest waves, no reflection and no transmission are observed, meaning that the plate dissipates all the incoming wave energy.

1976). Strong nonlinear behaviours can therefore be observed for waves that are far from the breaking limit. Several phenomena could be responsible for the plate changing its mean position. First, if a current takes place between the plate and the free surface, it could cause a depression similar to a Venturi effect. In such a configuration, Stokes drift could arise from wave steepness (Stokes 1847; Van den Bremer & Breivik 2018). In addition, waves above a rigid plate can lead to the creation of a mean flow (Carmigniani *et al.* 2017). The flow at the edge of the plate could explain the observations through its associated upward force. In the case of a rigid plate in a wave field, vortex creation has been reported
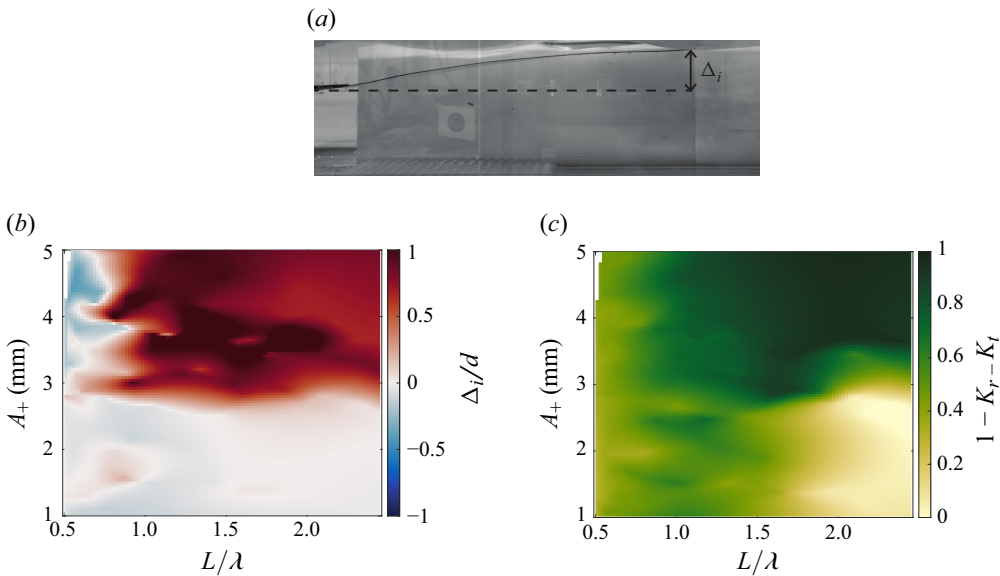
(*a*)

(*b*)

(*c*)

Figure 4. (*a*) Side view of the tank while sending waves of 6 mm amplitude with $L/\lambda = 0.99$. The plate tip is displaced from its initial position of Δ_i and reaches the free surface. (*b*) Plate tip mean displacement Δ_i normalized by plate depth d in an A_+ vs L/λ map. For the steepest waves, $\Delta_i \approx d$, meaning that the plate tip reaches the free surface. (*c*) The A_+ vs L/λ map of $1 - K_r - K_t$, meaning the part of the incoming wave energy that is dissipated by the interaction with the plate. Dissipation is maximum for the steepest waves.

by Boulier & Belorgey (1994), Poupardin *et al.* (2012) and Pinon *et al.* (2017). They observed that the vortex street has a given direction, slightly upward or downward. A similar phenomenon could exert a force upward on the plate tip.

Finally, this study opens questions regarding the origin of wave reflection by the plate. It appears that the reflection observed here cannot be completely predicted using a simple unique physical parameter. For instance, neither the plate length nor the plate resonance frequencies account for the reflection. Simulations, similar to the work of Shoele (2023) or Renzi (2016), could be efficient tools to examine this phenomenon through a wider exploration of the parameter space.

Declaration of interests. The authors report no conflict of interest.

REFERENCES

ACHOUR, N., MOUGEL, J., LO JACONO, D. & FABRE, D. 2020 Étude théorique de l'effet d'un faible courant sur les interactions houle/membrane flexible: application à la récupération d'énergie. In *XVI émes Journées Nationales Génie Côtier – Génie Civil Le Havre, 2020*, pp. 495–504. Editions Paralia CFL.

ALAM, M.-R. 2012 Nonlinear analysis of an actuated seafloor-mounted carpet for a high-performance wave energy extraction. *Proc. R. Soc. Lond. A: Math. Phys. Engng* **468** (2146), 3153–3171.

ASAEIAN, A., ABEDI, M., JAFARI-TALOOKOLAEI, R.-A. & ATTAR, M. 2020 Wave propagation through a submerged horizontal plate at the bottom of a water channel. *Comput. Engng Phys. Model.* **3** (4), 1–19.

BEHERA, H. 2021 Oblique wave scattering by a system of semi-infinite floating and submerged elastic plates. *Differ. Equ. Dyn. Syst.* **29** (1), 157–173.

BORAL, S., SAHOO, T. & MEYLAN, M.H. 2023 Gravity wave interaction with an articulated submerged plate resting on a winkler foundation. *Appl. Math. Model.* **113**, 416–438.

BOULIER, B. & BELORGEY, M. 1994 Ecoulement tourbillonnaire et zone d'affouillement générés par la houle en présence d'une plaque immergée. In *Actes des 3èmes Journées Nationales Génie Civil Génie Côitier, Sète, 24 mars 1994, thème 1*, p. 3945.

VAN DEN BREMER, T.S. & BREIVIK, Ø. 2018 Stokes drift. *Phil. Trans. R. Soc. Lond. A: Math. Phys. Engng Sci.* **376** (2111), 20170104.

CARMIGNIANI, R.A., BENOIT, M., VIOLEAU, D. & GHARIB, M. 2017 Resonance wave pumping with surface waves. *J. Fluid Mech.* **811**, 1–36.

CHO, I.H. & KIM, M.H. 2000 Interactions of horizontal porous flexible membrane with waves. *J. Waterway Port Coastal Ocean Engng* **126** (5), 245–253.

CHO, I.H. & KIM, M.H. 1998 Interactions of a horizontal flexible membrane with oblique incident waves. *J. Fluid Mech.* **367**, 139–161.

COLLINS, I., HOSSAIN, M., DETTMER, W. & MASTERS, I. 2021 Flexible membrane structures for wave energy harvesting: a review of the developments, materials and computational modelling approaches. *Renew. Sustain. Energy Rev.* **151**, 111478.

DAS, S., SAHOO, T. & MEYLAN, M.H. 2020 An investigation of the properties of flexural-gravity wave propagation in a coupled submerged and floating plate system. *Eur. J. Mech. B/Fluids* **82**, 123–134.

DESMARS, N., TCHOUFAG, J., YOUNESIAN, D. & ALAM, M.-R. 2018 Interaction of surface waves with an actuated submerged flexible plate: optimization for wave energy extraction. *J. Fluids Struct.* **81**, 673–692.

GAYATHRI, R., BENNY, C. & BEHERA, H. 2020 Wave attenuation by a submerged flexible permeable membrane. *AIP Conf. Proc.* **2277**, 210003.

GUO, Y.C., MOHAPATRA, S.C. & SOARES, C.G. 2020 Wave energy dissipation of a submerged horizontal flexible porous membrane under oblique wave interaction. *Appl. Ocean Res.* **94**, 101948.

KUMAR, P.S., MANAM, S.R. & SAHOO, T. 2007 Wave scattering by flexible porous vertical membrane barrier in a two-layer fluid. *J. Fluids Struct.* **23** (4), 633–647.

LE MÉHAUTÉ, B. 1976 *An Introduction to Hydrodynamics and Water Waves*. Springer Science & Business Media.

LEHMANN, M., ELANDT, R., PHAM, H., GHORBANI, R., SHAKERI, M. & ALAM, M.-R. 2013 An artificial seabed carpet for multidirectional and broadband wave energy extraction: Theory and experiment. In *Proceedings of 10th European Wave and Tidal Energy Conference*. Aalborg University.

MICHELE, S., BURIANI, F., RENZI, E., VAN ROOIJ, M., JAYAWARDHANA, B. & VAKIS, A.I. 2020 Wave energy extraction by flexible floaters. *Energies* **13** (23), 6167.

MIRZA, T. & HASSAN, M. 2024*a* A novel approach for using submerged structure as wave-trapping zone. *J. Fluid. Struct.* **129**, 104169.

MIRZA, T. & HASSAN, M. 2024*b* The study of water wave scattering by series of submerged elastic scatterers. *Phys. Fluids* **36** (8), 087111.

MOHAPATRA, S.C. & GUEDES SOARES, C. 2019 Interaction of ocean waves with floating and submerged horizontal flexible structures in three-dimensions. *Appl. Ocean Res.* **83**, 136–154.

MOHAPATRA, S.C & GUEDES SOARES, C. 2020 Hydroelastic response of a flexible submerged porous plate for wave energy absorption. *J. Mar. Sci. Engng* **8** (9), 698.

MOHAPATRA, S.C. & SAHOO, T. 2014 Wave interaction with a floating and submerged elastic plate system. *J. Engng Maths* **87** (1), 47–71.

MOISY, F., RABAUD, M. & SALSAC, K. 2009 A synthetic schlieren method for the measurement of the topography of a liquid interface. *Exp. Fluids* **46** (6), 1021–1036.

MORK, G., BARSTOW, S., KABUTH, A. & PONTES, M.T. 2010 Assessing the global wave energy potential. In *Proceedings of the ASME 2010 29th International Conference on Ocean, Offshore and Arctic Engineering. 29th International Conference on Ocean, Offshore and Arctic Engineering: Volume 3*, pp. 447–454. ASME.

OUELLET, Y. & DATTA, I. 1986 A survey of wave absorbers. *J. Hydraul. Res.* **24** (4), 265–280.

PINON, G., PERRET, G., CAO, L., POUPARDIN, A., BROSSARD, J. & RIVOALEN, E. 2017 Vortex kinematics around a submerged plate under water waves. Part II: Numerical computations. *Eur. J. Mech. B/ Fluids* **65**, 368–383.

POUPARDIN, A., PERRET, G., PINON, G., BOURNETON, N., RIVOALEN, E. & BROSSARD, J. 2012 Vortex kinematic around a submerged plate under water waves. Part I: Experimental analysis. *Eur. J. Mech. B/ Fluids* **34**, 47–55.

RENZI, E. 2016 Hydroelectromechanical modelling of a piezoelectric wave energy converter. *Proc. R. Soc. Lond. A: Math. Phys. Engng Sci.* **472** (2195), 20160715.

SHENG, W. 2019 Wave energy conversion and hydrodynamics modelling technologies: a review. *Renew. Sustain. Energy Rev.* **109**, 482–498.

SHOELE, K. 2023 Hybrid wave/current energy harvesting with a flexible piezoelectric plate. *J. Fluid Mech.* **968**, A31.

STAMOS, D.G. & HAJJ, M.R. 2001 Reflection and transmission of waves over submerged breakwaters. *J. Engng Mech.* **127** (2), 99–105.

STOKES, G.G. 1847 On the theory of oscillatory waves. *Trans. Camb. Phil. Soc.* **8**, 441–455.

URSELL, F. 1952 Edge waves on a sloping beach. *Proc. R. Soc. Lond. A: Math. Phys. Engng Sci.* **214** (1116), 79–97.

WILDEMAN, S. 2018 Real-time quantitative Schlieren imaging by fast Fourier demodulation of a checkered backdrop. *Exp. Fluids* **59** (6), 1–13.